Spectrum of a Gross-Neveu Yukawa model with flavor disorder in three dimensions

Shiroman Prakash*

Dayalbagh Educational Institute, Agra 282005, India

(Received 31 January 2023; accepted 27 February 2023; published 28 March 2023)

We show that a variant of the Gross-Neveu Yukawa model with disorder provides a real, non-supersymmetric generalization of the Sachdev–Ye Kitaev (SYK) model to three dimensions. The model contains M real scalar fields and N Dirac (or Majorana) fermions, interacting via a Yukawa interaction with a local Gaussian random coupling in three dimensions. In the limit where M and N are both large, and the ratio M/N is held fixed, the model defines a line of infrared fixed points parametrized by M/N, reducing to the Gross-Neveu vector model when $M/N = 0$. When M/N is nonzero, the model is dominated by melonic diagrams and gives rise to SYK-like physics. We compute the spectrum of single-trace operators in the theory, and find that it is real for all values of M/N.

DOI: 10.1103/PhysRevD.107.066025

I. INTRODUCTION

The large-N limit [1] is a powerful tool to understand strongly interacting quantum field theories. In this limit, unexpected, classical descriptions can emerge—the most notable example of which is classical gravity in anti–de Sitter space [2–4].

Originally, two large-N limits were known—the large-N limit of theories with dynamical fields in adjoint/matrix representations, exemplified by [1], in which all planar Feynman diagrams contribute; and theories with dynamical fields in the vector representation, exemplified by [5], in which a summable subset of planar Feynman diagrams contributes. Large N vector models typically possess a slightly broken higher-spin symmetry, and any dual gravitational description for such a conformal field theory (CFT) would include a tower of massless higher-spin gauge fields [6–12]. On the other hand, strongly interacting large-N matrix models are, at least in some cases with sufficient supersymmetry [2,13], believed to be dual to theories of Einstein supergravity.

Theories also exist whose large-N limit interpolates between a vector model and a matrix model. The Aharony-Bergman-Jafferis (ABJ) theory [14] is a bifundamental $U(N) \times U(M)$ Chern-Simons theory that can be studied in the limit where M and N are both large and the ratio M/N is fixed. When $M/N \ll 1$, the theory possesses a slightly broken higher-spin symmetry and is effectively a vector model, dual to a higher-spin gauge theory [with $U(M)$ Chan-Paton indices] [15]. When $M/N = 1$, the theory becomes Aharony-Bergman-Jafferis-Maldacena (ABJM) theory [13] and is dual to type-IIA supergravity in $\mathrm{AdS}_4 \times CP_3$ at strong coupling. The parameter M/N can be understood as a gravitational 't Hooft coupling in the bulk; as this parameter is increased from zero to one, the higher-spin gauge fields somehow coalesce into strings.

Large N vector model CFTs without supersymmetry are common. Do there exist large-N CFTs without supersymmetry dual to Einstein gravity in AdS? A variant of the weak gravity conjecture [16] suggests that the answer is no. However, motivated by ABJ [15], one may promote non-supersymmetric vector models to bifundamental theories, and study their behavior as a function of M/N [17,18]. However, all examples studied so far become complex at some critical value of M/N, as can be seen via the epsilon expansion [18,19], or, in the case of certain matter Chern-Simons theories [17,20], cannot be studied at strong coupling.

Recently, a new large-N limit—the melonic limit[1]—has emerged, via the study of the Sachdev–Ye Kitaev (SYK) model [31–35], a chaotic model in one dimension, exhibiting features of black hole physics, see, e.g., [36–42]. The melonic limit is dominated by a summable subset of planar diagrams that manages to capture nontrivial aspects of gravitational physics. Does there exist a nonsupersymmetric higher-dimensional generalization of the SYK model [43–48]? All nonsupersymmetric

*Corresponding author.
sprakash@dei.ac.in

[1]This limit was first understood via tensor models, e.g., [21–30].

constructions [44,45,48] encounter an operator with a complex scaling dimension. Similar results have also been observed in tensor models, [29,49–51]. In particular [48], inspired by [46], defined a "biconical" SYK model that interpolates between the critical $O(N)$ vector model when $M/N \ll 1$ and a model with SYK-like physics when M/N is finite. Their model becomes complex when M/N exceeds 0.22, reminiscent of bifundamental critical scalars in $d = 3$ [18,19]. By contrast, [48] shows that a supersymmetric version of their theory is real for all M/N.

It is natural to expect that nonsupersymmetric melonic CFTs do not exist—and, if this were true, it would provide strong support for the conjecture that nonsupersymmetric strongly interacting CFT's dominated by planar diagrams do not exist. Here, we show that this expectation is false by computing the spectrum a simple example of a nonsupersymmetric CFT, recently proposed in [52], dominated by melonic diagrams that can be studied for all values of M/N.

II. GROSS-NEVEU YUKAWA MODEL WITH DISORDER

A starting point in a search for higher-dimensional SYK physics is the Gross-Neveu (GN) model [53], which possesses a nontrivial ultraviolet fixed point in $d = 2 + \epsilon$, that, at least when N is large, defines a conformal field theory in $d = 3$. A tensorial GN model was constructed in [50,54,55], but its spectrum of operators includes one with a complex dimension—an identical spectrum arises in a GN model with a random four-fermion interaction. However, there exists a cousin of the GN model—the Gross-Neveu Yukawa (GNY) model [56–59]—that gives rise to an *infrared* fixed point in $d = 4 - \epsilon$, equivalent to the GN fixed point when N is large [58,59]. See, e.g., [60–77] for more on the GN and GNY theories.

Inspired by [48], we study a variant of the GNY model constructed by [52]. The model, which is closely related to several one-dimensional models generalizing SYK [78–83], consists of M real scalar fields, σ^a, $a = 1, \ldots, M$, and N Dirac or Majorana fermions, ψ^i, $i = 1, \ldots, N$ with the interaction,

$$\mathcal{S}_{\text{int}} = \int d^d x g_{ai}{}^j \sigma^a \bar{\psi}^i \psi_j, \tag{1}$$

which is relevant for $d < 4$, and leads to an IR fixed point in $d = 3$.

$g_{ai}{}^j$ is a random coupling with quenched disorder, with zero mean $\langle g_{ai}{}^j \rangle = 0$, but nonzero variance

$$\langle g_{ai}{}^j g_{bk}{}^l \rangle = \frac{J}{N^2} \delta_{ab} \delta_i^l \delta_k^j. \tag{2}$$

The resulting average is invariant under $O(M) \times U(N)$ for the theory with Dirac fermions [or $O(M) \times O(N)$ for Majorana fermions].

We take both M and N to be large, keeping the ratio $\lambda = \frac{M}{N}$ fixed. It follows from [84] that this limit is dominated by melonic diagrams.

When $\lambda = 0$, the theory reduces to the GN model, but it exhibits SYK-like physics for M/N finite.

Does the spectrum of single-trace primaries, like all other known nonsupersymmetric, higher-dimensional melonic models, include a complex scaling dimension for M/N sufficiently large? We compute the spectrum in $d = 3$, and find it is real for all values of M/N.

We present the spectrum for the theory with N Dirac fermions below—the spectrum of the theory with $2N$ Majorana fermions is a truncation to operators with even spin.

III. EXACT PROPAGATORS

The exact propagators for ψ and σ were obtained in [52], as we review below.

Denote the exact propagators by

$$\begin{aligned} \langle \psi^i(p) \bar{\psi}_j(-q) \rangle &= (2\pi)^d G(p) \delta^d(p-q) \delta^i_j, \\ \langle \sigma^a(p) \sigma^b(-q) \rangle &= (2\pi)^d G(p) \delta^d(p-q) \delta^{ab}. \end{aligned} \tag{3}$$

In the melonic limit, these propagators satisfy the Schwinger-Dyson equations illustrated in Fig. 1,

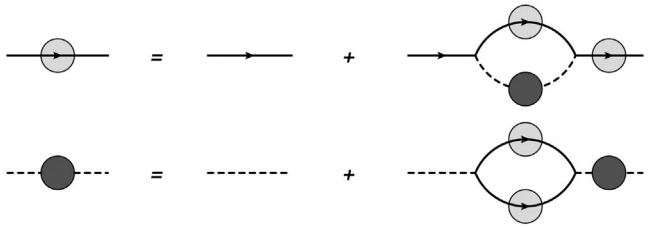

FIG. 1. The Schwinger-Dyson equations for the exact propagators. Solid and dashed lines denote fermion and scalar propagators, respectively.

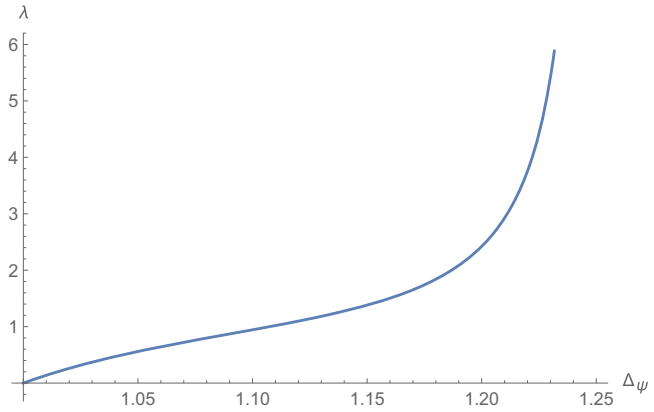

FIG. 2. The gap equation for Δ_ψ in $d = 3$ possesses a unique solution for all λ.

$$F_0(p)^{-1} = F(p)^{-1} - J\int \frac{d^d q}{(2\pi)^d}\mathrm{tr}\ \left(G(q)G(p+q)\right) \tag{4}$$

$$G_0(p)^{-1} = G(p)^{-1} + J\lambda\left(\int \frac{d^d q}{(2\pi)^d} G(p-q)F(q)\right), \tag{5}$$

where $G_0(p) = \frac{1}{i\not{p}}$ and $F_0(p) = \frac{1}{p^2}$.

The conformal ansatz for interacting propagators in the IR is

$$G(p) = A\frac{i\not{p}}{p^{d-2\Delta_\psi+1}}, \qquad F(p) = \frac{B}{p^{d-2\Delta_\sigma}}. \tag{6}$$

For an interacting IR solution, we require

$$2\Delta_\psi + \Delta_\sigma = d, \tag{7}$$

and

$$(d+2)/4 > \Delta_\psi > (d-1)/2. \tag{8}$$

Evaluating Eqs. (4) and (5) using (6), we obtain an equation that determines Δ_ψ, which, in $d = 3$, reads

$$\lambda = \frac{8(2\Delta_\psi - 5)(2\Delta_\psi - 3)\sin^3(\pi\Delta_\psi)\cos(\pi\Delta_\psi)\Gamma(3-4\Delta_\psi)\Gamma(4\Delta_\psi - 4)}{\pi}. \tag{9}$$

Figure 2 shows that, in $d = 3$, (9) has a unique solution within the allowed range, for all λ. For small λ,

$$\Delta_\psi = 1 + \frac{2\lambda}{3\pi^2} + \frac{80\lambda^2}{27\pi^4} - \frac{(120\pi^2 - 4384)\lambda^3}{243\pi^6} + O(\lambda^4). \tag{10}$$

This agrees with the $O(1/N)$ correction to $\Delta\psi$ in the GN model.

As $\lambda \to \infty$, $\Delta_\psi \to 5/4$ and $\Delta_\sigma \to 1/2$. In between, there is a "critical value" of $\lambda_* = \frac{2(d-1)d_\gamma}{d+2} = \frac{8}{5}$ defined by the condition $2\Delta_\sigma = 2\Delta_\psi - 1$, for which $\Delta_\sigma = 2/3$ and $\Delta_\psi = 7/6$.

Does the free theory flow to this putative IR limit? In Appendix A we solved the full gap equations (4) and (5), for $\lambda = 0$ and $\lambda = \infty$, and found flows from the free theory to the IR solution. Presumably, similar flows also exist for intermediate values of λ.

IV. OPERATOR SPECTRUM

The single-trace primaries are bilinear singlets of the $O(M) \times U(N)$ symmetry group.[2] In the free theory, these are

(1) spin-s bilinears of ψ, of the schematic form, $\bar\psi^i(\partial\cdot\gamma)^n\psi_i$, for $s = 0$, and, $\bar\psi^i\gamma\cdot z(\partial\cdot z)^{s-1}(\partial\cdot\gamma)^n\psi_i$, for $s > 0$;

(2) and (even) spin-s bilinears of σ, of the schematic form

$$\sigma^a(\partial\cdot z)^s(\partial^{2m})\sigma^a.$$

[2]Note that bilinears such as $\sigma_a\psi_i$ or, more generally $\sigma_a A^{ai}\psi_i$, for any $M \times N$ matrix A, are not invariant under the $O(M) \times U(N)$ symmetry group—anomalous dimensions of such operators are suppressed by $1/N$.

Here, z denotes a null polarization vector (see, e.g., [85,86]). In the IR fixed point, fermion and scalar bilinears which are parity even can mix.

Let $\mathcal{O}_{s,\tau}$ be an operator with well-defined scaling dimension, and let $\tau = \Delta_\mathcal{O} - s$ be its twist. In the IR limit, the three-point functions $\langle\sigma(x_1)\sigma(x_2)\mathcal{O}_{\tau,s}(x_3)\rangle$ and $\langle\psi(x_1)\bar\psi(x_2)\mathcal{O}_{\tau,s}(x_3)\rangle$ satisfy the melonic ladder equation, shown schematically in Fig. 3. Following [87], we use this equation, along with conformal invariance, to determine the allowed operator spectrum in the IR. Details are in Appendix B.

Figure 3 translates into a condition that an integration kernel (which is, in general, a matrix, due to mixing and multiple allowed forms for conformally invariant three-point functions), $\mathbf{K}_s^{\mathrm{even/odd}}(\Delta)$, defined for parity-even/odd spin-s operators, has eigenvalue 1.

V. SPECTRUM IN $d = 3$

We now show that the spectrum of single-trace operators is real for all λ in $d = 3$. As usual for SYK-like models, the results involve some numerical solutions of transcendental equations. Alternatively, analytic expressions for the

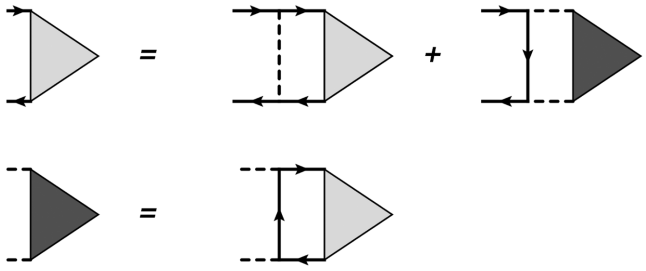

FIG. 3. In the melonic IR limit, the exact three-point functions $\langle\sigma(x_1)\sigma(x_2)\mathcal{O}_{\tau,s}(x_3)\rangle$ and $\langle\psi(x_1)\bar\psi(x_2)\mathcal{O}_{\tau,s}\rangle(x_3)$ (depicted as dark and light gray triangles) satisfy the ladder equation depicted. All propagators are exact.

spectrum can be obtained in $d = 4 - \epsilon$, which are presented in Appendix D.

A. Parity-odd scalars

We expect the scaling dimensions of parity-odd scalars, denoted as $\tilde{\Delta}_n$, to take the form $\tilde{\Delta}_n = 2\Delta_\psi + 2n + \tilde{\gamma}_{0,n}$, with $\tilde{\gamma}_{0,n} \to 0$ as $n \to \infty$.

Figure 3 translates into the equation

$$K_0^{\text{odd}}(\tilde{\Delta}) = 1, \tag{11}$$

as described in Appendix B.

For $\lambda = 1$, we find $\tilde{\Delta}_n = 2.53354,\ 4.25934,\ 6.23292,\ 8.22512,\ldots$, approaching $2\Delta_\psi + 2n = 2.21492 + 2n$. For $\lambda = \infty$, we find $\tilde{\Delta}_n = 2.85171, 4.66395, 6.60305, 8.57464, \ldots$, also approaching $2\Delta_\psi + 2n = 2.5 + 2n$. The behavior for intermediate values of λ is similar, and the spectrum is *real* for all values of λ. The scaling dimension of the lowest-dimension parity-odd scalar is shown in Fig. 4. In the melonic GN model [50], this operator has a complex scaling dimension.

For small λ,

$$\begin{aligned}\tilde{\Delta}_0 &= 2 + \frac{16}{3\pi^2}\lambda - \frac{128}{27\pi^4}\lambda^2 + O(\lambda^3) \\ &= 2\Delta_\psi + \frac{4\lambda}{\pi^2} + O(\lambda^2),\end{aligned} \tag{12}$$

$$\begin{aligned}\tilde{\Delta}_n = 2\Delta_\psi + 2n &+ \frac{16}{3\pi^4 n(2n+1)}\lambda^2 \\ &+ \left(\frac{192(\log 2n + \gamma + 2) + 32}{27\pi^6 n^2} + O\left(\frac{1}{n^3}\right)\right)\lambda^3 \\ &+ O(\lambda^4).\end{aligned} \tag{13}$$

At large n,

$$\tilde{\gamma}_{0,n} \sim \frac{1}{n^{2\Delta_\sigma}}. \tag{14}$$

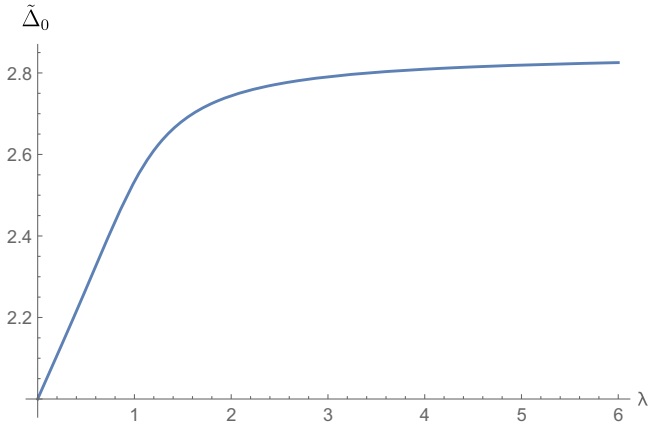

FIG. 4. Scaling dimension of the lowest-twist parity-odd scalar, $\bar{\psi}\psi$, as a function of λ.

B. Parity-even scalars

The spectrum of parity-even scalars includes mixtures of scalar and fermion bilinears, operators, denoted as type-A and type-B, whose scaling dimensions are of the form $\Delta_n^A = 2\Delta_\psi + 2n + 1 + \gamma_{0,n}^A$ and $\Delta_n^B = 2\Delta_\sigma + 2n + \gamma_{0,n}^B$, respectively, where $\gamma_{0,n}^{A/B} \to 0$ as $n \to \infty$.

Due to mixing, the integration kernel for parity-even scalars is a 2×2 matrix, $\mathbf{K}_0^{\text{even}}(\Delta)$, given in (B13) in Appendix B.

The condition

$$\det\left(\mathbf{K}_0^{\text{even}}(\Delta) - \mathbf{1}\right) = 0 \tag{15}$$

determines the allowed values of Δ.

We find the spectrum for $\lambda = 1$ is 2.37666, 3, 3.70347, 5.23918, 5.57576, 7.22808, 7.57099,.... The scaling dimension of the lowest operator is plotted as a function of λ in Fig. 5.[3]

We plot the scaling dimensions of the eight lowest scalar primaries in Fig. 6. As Fig. 6 illustrates, the spectrum is real for all values of λ. As $n \to \infty$, the scaling dimensions approach $2\Delta_\sigma + 2n$ and $2\Delta_\psi + 2n + 1$.

There exists an exactly marginal operator with $\Delta = 3$, for all λ. We expect that this corresponds to a mixture of $\sigma^a \partial^2 \sigma^a$ and $\bar{\psi}^i \not{\partial} \psi_i$, which is redundant and vanishes by the equation of motion. as in [41,88].

For small λ,

$$\Delta_0^A = 3, \tag{16}$$

$$\begin{aligned}\Delta_n^A = 2\Delta_\psi + 2n + 1 &+ \frac{16(2n^2 + 3n - 1)}{3n(4n^3 + 12n^2 + 11n + 3)}\frac{\lambda^2}{\pi^4} \\ &+ \left(\frac{192(\log 2n + \gamma + 2) + 32}{27\pi^6 n^2} + O\left(\frac{1}{n^3}\right)\right)\lambda^3 \\ &+ O(\lambda^4) \quad \text{for } n > 0,\end{aligned} \tag{17}$$

$$\Delta_0^B = 2\Delta_\sigma + \frac{8\lambda}{\pi^2} + \frac{(14208 - 928\pi^2)\lambda^3}{27\pi^6} + O(\lambda^4) \tag{18}$$

and

$$\begin{aligned}\Delta_n^B = 2\Delta_\sigma + 2n &+ \frac{64}{3\pi^4 n(n+1)(2n-1)(2n+1)}\lambda^2 \\ &+ \left(-\frac{384(\log 2n + \gamma - 4) + 128}{27\pi^6 n^4} + O\left(\frac{1}{n^5}\right)\right)\lambda^3 \\ &+ O(\lambda^4) \quad \text{for } n > 0.\end{aligned} \tag{19}$$

[3]Both the lowest scaling dimension Δ_0 and its shadow $\Delta_0' = 3 - \Delta_0$ are above the unitary bound for all λ. Our analysis does not determine which is realized in the IR limit; however, as $\lambda \to 0$, $\Delta_0 \to 2^+ = 2\Delta_\sigma$, in agreement with the GN model. Assuming the spectrum is a continuous function of λ, we conclude Δ_0 is the scaling dimension in the IR.

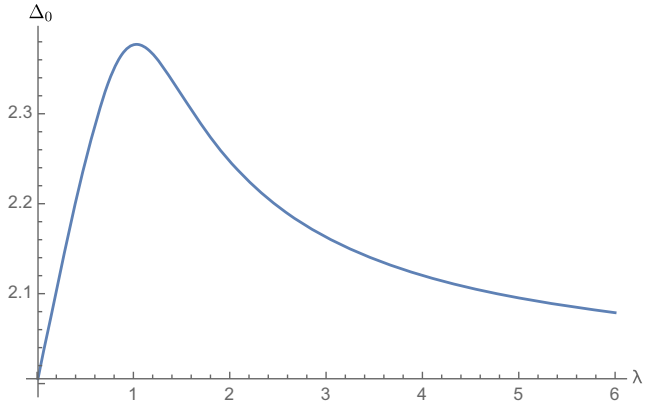

FIG. 5. The scaling dimension $\Delta_0(\lambda)$ of the lowest-dimension parity-even scalar as a function of λ. $\Delta(\lambda)$ attains its maximum, 2.377 near $\lambda = 1.03$.

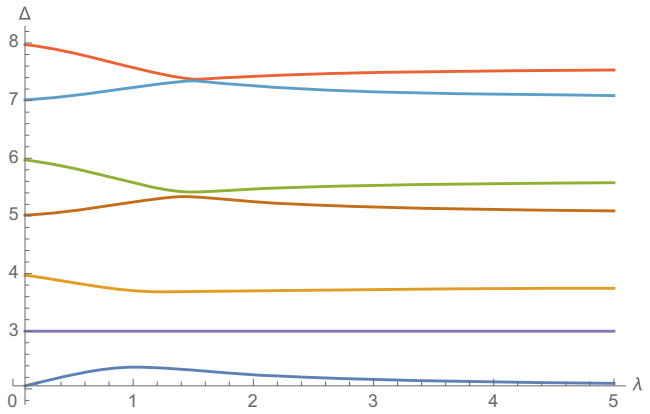

FIG. 6. The lowest eight scaling dimensions of parity-even scalars a function of λ. $\Delta_0(\lambda)$ attains its maximum, 2.377 near $\lambda = 1.03$. The kink in the graphs is, for large n, near $\lambda = 8/5$.

The order λ contribution to operators for which $n > 0$ vanishes (for both type-A and type-B), as expected, since these are double-trace operators in the theory when $M = 1$.

When n is large,

$$\lim_{n\to\infty} \gamma_n^A \sim n^{-2\Delta_\sigma}, \tag{20}$$

and

$$\lim_{n\to\infty} \gamma_n^B \sim \begin{cases} n^{-4\Delta_\psi} & \lambda \neq 8/5 \\ n^{-10/3} & \lambda = 8/5. \end{cases} \tag{21}$$

C. Leading-twist higher-spin operators

We next present the spectrum of leading-twist higher-spin operators, i.e., those which become almost-conserved currents when $\lambda \to 0$.

The twists of such operators, which are all parity even, solve an equation of the form

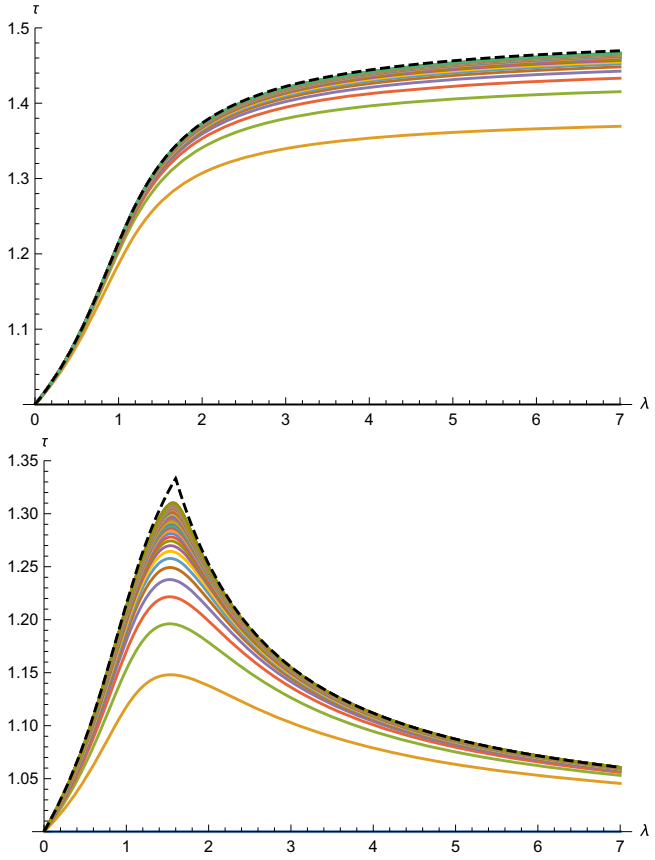

FIG. 7. The spectrum of leading-twist operators of spin s, for s odd (above) and even (below), is shown for $s = 1, \ldots, 80$. As $s \to \infty$, the twists approach the dashed line, and, for even spins, peak near $\lambda = 8/5$.

$$\det\left(\mathbf{K}_s^{\text{even}}(\tau) - \mathbf{1}\right) = 0, \tag{22}$$

where $\mathbf{K}_s^{\text{even}}(\tau)$ is given in Appendix B.

The resulting twists are shown in Fig. 7. For all λ, there exists a twist-1 spin-1 and spin-2 operator, corresponding to the conserved $U(1)$ current and stress tensor.

For odd spins,

$$\lim_{s\to\infty} \tau_s^{\min} = 2\Delta_\psi - 1, \tag{23}$$

while for even spins,

$$\lim_{s\to\infty} \tau_s^{\min} = \begin{cases} 2\Delta_\psi - 1 & \lambda \leq 8/5 \\ 2\Delta_\sigma & \lambda > 8/5. \end{cases} \tag{24}$$

Define

$$\gamma_s = \tau_s - \lim_{s\to\infty} \tau_s^{\min}. \tag{25}$$

For small λ,

$$\gamma_s = \begin{cases} -\frac{4\lambda}{\pi^2(2s-1)} + \frac{16(4s(2s-1)^2 H_{s-1} - (2s-1)^2(2s+1)(H_{s-\frac{3}{2}} + 2\log 2) - 2s(16s^2-22s+13))}{3\pi^4(2s-1)^3(2s+1)}\lambda^2 + O(\lambda^3) & s \text{ even} \\ -\frac{4\lambda}{\pi^2(4s^2-1)} - \frac{16((1-4s^2)^2(H_{s-\frac{3}{2}} + 2\log(2)) + 2(20s^4-13s^2+6s+2))}{3\pi^4(4s^2-1)^3}\lambda^2 + O(\lambda^3) & s \text{ odd.} \end{cases} \tag{26}$$

For s large and even,

$$\gamma_s \sim \begin{cases} -\frac{\cos(\pi\Delta_\psi)\Gamma(\frac{7}{2}-3\Delta_\psi)\Gamma(\frac{7}{2}-\Delta_\psi)\Gamma(2\Delta_\psi-\frac{3}{2})}{\pi^{3/2}(4(\Delta_\psi-2)\Delta_\psi+3)\Gamma(3-4\Delta_\psi)} s^{1-2\Delta_\psi} & \lambda < 8/5 \\ -\frac{9\sqrt{\frac{3}{55}}\Gamma(\frac{8}{3})\Gamma(\frac{14}{3})}{4\cdot 2^{5/6}\pi} s^{-2/3} & \lambda = 8/5 \\ \frac{2\sin(4\pi\Delta_\psi)\cos(\pi\Delta_\psi)\Gamma(3-2\Delta_\psi)\Gamma(\frac{7}{2}-\Delta_\psi)\Gamma(2\Delta_\psi-\frac{1}{2})\Gamma(3\Delta_\psi-\frac{7}{2})}{\pi^{5/2}(2\Delta_\psi-1)} s^{1-2\Delta_\psi} & \lambda > 8/5. \end{cases} \tag{27}$$

The asymptotic behavior at $\lambda = 8/5$ is unusual—at $\lambda = 8/5$, $\Delta_\sigma = \frac{2}{3}$ is the smallest twist in the theory. For s odd, we find

$$\gamma_s \sim -\frac{2(5-2\Delta_\psi)^2\sin^2(2\pi\Delta_\psi)\Gamma(3-2\Delta_\psi)\Gamma(4-2\Delta_\psi)}{\pi^2(2\Delta_\psi-1)^2}(4s)^{-2\Delta_\sigma}. \tag{28}$$

The subleading contribution is $s^{2\Delta_\psi-4} = s^{-(\Delta_\sigma+1)}$, which is numerically close to the leading contribution for $1 < \Delta_\psi < 5/4$. In the limit $\lambda \to 0$, both the leading and subleading terms approach $s^{-2+O(\lambda)}$.

The spectrum of both parity-odd and -even higher-twist, higher-spin operators are also real for all λ, and are presented in Appendix C.

D. Conformal Regge limit

As explained in [44], if we continue the function $\Delta(s)$ that encodes the scaling dimensions of leading-twist operators of spin s to complex spins, the value of s_* that solves $\Delta(s_*) = \frac{3}{2}$ can be used to extract the Lyapunov exponent in a particular hyperbolic geometry via $\lambda_{\text{hyp}} = s_* - 1$. The result[4] is shown in Fig. 8, and is similar to [48].

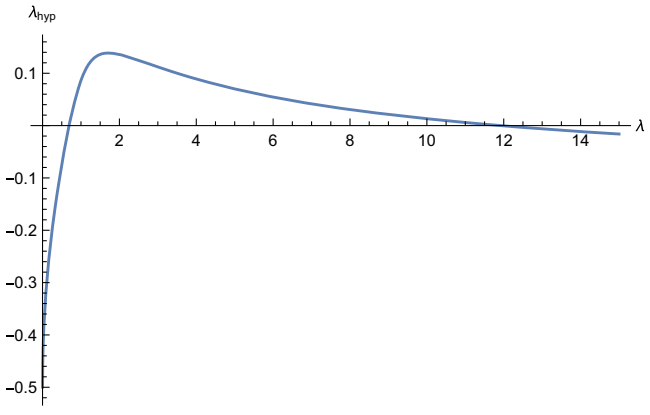

FIG. 8. The even-spin hyperbolic Lyapunov exponent $\lambda_{\text{Hyp}} = s_* - 1$ as a function of λ. The maximum of $\lambda_{\text{hyp}} = 0.139$ is attained at $\lambda = 1.71$.

VI. DISCUSSION

In this paper, we showed that the spectrum of single-trace operators in an IR fixed point defined via a disordered Gross-Neveu Yukawa model is real for all values of M/N. This strongly suggests the model is the first real, non-supersymmetric CFT in $d > 1$ that admits an SYK-like large-N limit. Moreover, the theory is a rare example of a solvable, nonsupersymmetric interacting large-N CFT in three dimensions.

Several questions exist for further research.

When $M/N = 0$, the CFT is dual to a higher-spin gauge theory [7]. Is the theory at finite M/N dual to a deformation of this higher-spin gauge theory?

Our results also suggest that a bifundamental Gross-Neveu Yukawa model, without disorder, could perhaps define a real planar large-N CFT in $d = 3$.

Disordered models with Yukawa interactions [80,81,89–91] and certain coupled SYK/tensor models [92,93] have been studied as toy models for superconductivity. The model studied here does not exhibit $U(1)$ symmetry breaking, but may perhaps be generalized to one which does.

We hope to return to these questions in the near future.

ACKNOWLEDGMENTS

The author thanks I. Klebanov, R. Loganayagam, S. Minwalla, M. Rangamani, R. Sinha and S. Sachdev for

[4]This computation uses the analytically continued spectrum $\Delta(s)$ of leading-twist, parity-even operators of even spin.

discussions and comments on a draft of this publication. The author also thanks International Centre for Theoretical Sciences, Bengaluru, for hospitality where part of this work was completed. The author is supported in part by DST Grants No. MTR/2018/0010077 and No. CRG/2021/009137.

APPENDIX A: SOLVING THE GAP EQUATION FROM UV TO IR

In this Appendix, we solve the gap equation from weak to strong coupling for $M \ll N$ very small, and $M \gg N$. From these results it seems natural to expect that a flow also exists for intermediate values of M/N.

Let $F(p) = 1/f(p)$ and $G(p) = -ip/g(p)$. Note that $[J] = 1$ in $d = 3$, so we expect these to be functions of the dimensionless quantity p/J.

The gap equations are

$$f(p) = p^2 - Jd_\gamma \int \frac{d^d q}{(2\pi)^d} \frac{q^2 + q\cdot p}{g(q)g(p+q)} \tag{A1}$$

$$g(p) = p^2 + J\lambda \int \frac{d^d q}{(2\pi)^d} \frac{p\cdot q}{g(q)f(p-q)}. \tag{A2}$$

We will show these equations have a solution interpolating from the free UV solution to the IR solution at the extreme values of λ, $\lambda = 0$ and $\lambda = \infty$, which are easier to handle than intermediate values of λ. We have not attempted to numerically solve the gap equation for general λ.

The $\lambda = 0$ solution is trivial, and can be obtained analytically. We have $g^{(\lambda=0)}(p) = p^2$, and $f^{(\lambda=0)}(p)$ is given by

$$f^{(\lambda=0)}(p) = p^2 - Jd_\gamma \int \frac{d^d q}{(2\pi)^d} \frac{q^2 + q\cdot p}{q^2(p+q)^2} \tag{A3}$$

$$= p^2 - d_\gamma J \frac{2^{-d}\pi^{1-\frac{d}{2}} \csc(\frac{\pi d}{2})\Gamma(\frac{d}{2})}{\Gamma(d-1)} p^{d-2} \tag{A4}$$

$$\to_{d\to 3} p^2 + \frac{J}{8} p. \tag{A5}$$

For $\lambda \to \infty$, we must solve the gap equation numerically. Let $\tilde{J} = \lambda J$. Then $f^{(\lambda=\infty)}(p) = p^2$, and $g^{(\lambda=\infty)}(p)$ satisfies

$$g^{(\lambda=\infty)}(p) = p^2 + \tilde{J} \int \frac{d^3 q}{(2\pi)^3} \frac{p\cdot q}{g^{(\lambda=\infty)}(p)(p-q)^2}. \tag{A6}$$

which we can write as

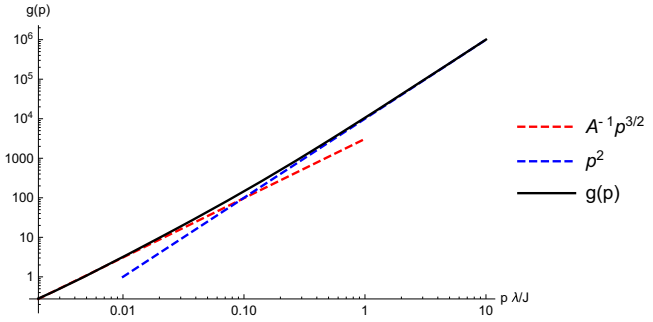

FIG. 9. A numerical solution of the gap equation from UV to IR, for the case of $\lambda \to \infty$ is shown above (the solid black line). It interpolates from $g(p) \sim A^{-1}p^{3/2}$ (dashed red line) to $g(p) \sim p^2$ (dashed blue line) as expected.

$$g^{(\lambda=\infty)}(p) = p^2 + \frac{\tilde{J}}{p(2\pi)^2} \int_0^\infty \frac{q^3 dq}{g^{(\lambda=\infty)}(p)} \mathcal{F}(q/p), \tag{A7}$$

where

$$\mathcal{F}(q) = \int_{-1}^{1} dt \frac{t}{1+q^2-2qt}. \tag{A8}$$

We solve this equation iteratively, choosing the initial seed function as $g_{\text{seed}}(p) = p^2 + A^{-1}p^{3/2}$, where $A^2 = \frac{10\pi}{3\tilde{J}}$. Within a few iterations, this converged to the numerical function plotted in Fig. 9.

APPENDIX B: DETAILS OF THE COMPUTATION OF THE SPECTRUM

1. Conformally invariant three-point functions

Let $\mathcal{O}^{\text{odd/even}}_{\tau,s}(x,z)$ be a parity-odd/parity-even operator with spin s and twist $\tau = \Delta_{\mathcal{O}} - s$. There are two allowed forms [85] for conformally invariant three-point correlation functions,

$$\langle \bar{\lambda}_1 \psi(x_1) \mathcal{O}^{\text{odd/even}}_{\tau,s}(x_3,z_3) \bar{\psi}(x_2)\lambda_2\rangle,$$

which are

$$\langle \bar{\lambda}_1 \psi(x_1) \mathcal{O}^{\text{odd}}_{\tau,s}(x_3,z_3) \bar{\psi}(x_2)\lambda_2\rangle = \frac{1}{x_{31}^\tau x_{12}^{2\Delta_\psi - 1-\tau} x_{23}^\tau} (b_1 (S_3/P_3) Q_3^s + b_2 (S_1/P_1) P_2 Q_3^{s-1}), \tag{B1}$$

for parity-odd operators, and

$$\langle \bar{\lambda}_1 \psi(x_1) \mathcal{O}^{\text{even}}_{\tau,s}(x_3,z_3) \bar{\psi}(x_2)\lambda_2\rangle = \frac{1}{x_{31}^\tau x_{12}^{2\Delta_\psi - 1-\tau} x_{23}^\tau} (a_1 P_3 Q_3^s + a_2 P_1 P_2 Q_3^{s-1}), \tag{B2}$$

for parity-even operators. Here Q_i, P_i and S_i are defined in [85], as

$$P_3 = \bar{\lambda}_1 \frac{\not{x}_{12}}{x_{12}^2}\lambda_2, \qquad Q_3 = 2z_3 \cdot \left(\frac{x_{32}}{x_{32}^2} - \frac{x_{31}}{x_{31}^2}\right),$$
$$S_3/P_3 = i\bar{\lambda}_2 \not{x}_{23}\not{x}_{31}\lambda_1/(|x_{12}||x_{23}||x_{31}|). \tag{B3}$$

For $s = 0$, the second term in each of the two above expressions should be omitted, and there is only one allowed form for the three-point function.

The correlation function $\langle\sigma(x_1)\sigma(x_2)\mathcal{O}^{\text{odd}}_{\tau,s}\rangle$ vanishes. The only allowed form for a conformally invariant correlation function $\langle\sigma(x_1)\sigma(x_2)\mathcal{O}^{\text{even}}_{\tau,s}(x_3, z_3)\rangle$ is

$$\langle\sigma(x_1)\sigma(x_2)\mathcal{O}^{\text{even}}_{\tau,s}(x_3)\rangle = \frac{c_1 Q_3^s}{x_{12}^{2\Delta_\sigma-\tau}x_{23}^{\tau}x_{31}^{\tau}}. \tag{B4}$$

It is convenient to take the limit $x_3 \cdot z_3 = 0$ and $x_3 \to \infty$, which can be obtained by a conformal transformation. This makes $Q_3 \to 2z_3 \cdot \frac{x_{21}}{x_3^2}$ We also rescale the correlation functions by a factor of $x_3^{2\tau+2s}$. In this limit the allowed forms for the correlation functions become

$$v_{a_1} = \bar{\lambda}_1 \not{x}_{12}\lambda_2 \frac{(x_{12}\cdot\epsilon)^s}{|x_{12}|^{-\tau+1+2\Delta_\psi}} \tag{B5}$$

$$v_{a_2} = \bar{\lambda}_1 \not{\epsilon}\lambda_2 \frac{(x_{12}\cdot\epsilon)^{s-1}}{|x_{12}|^{-\tau-1+2\Delta_\psi}} \tag{B6}$$

$$v_{b_1} = \bar{\lambda}_1\lambda_2 \frac{(x_{12}\cdot\epsilon)^s}{|x_{12}|^{2\Delta_\psi-\tau}} \tag{B7}$$

$$v_{b_2} = \bar{\lambda}_1 \not{\epsilon}\not{x}_{12}\lambda_2 \frac{(x_{12}\cdot\epsilon)^{s-1}}{|x_{12}|^{2\Delta_\psi-\tau}} \tag{B8}$$

$$v_{c_1} = \frac{(x_{12}\cdot\epsilon)^s}{|x_{12}|^{2\Delta_\sigma-\tau}}. \tag{B9}$$

We may prefer to choose a different basis for the parity-odd three-point functions, by defining

$$v'_{b_2} = \bar{\lambda}_1(\not{\epsilon}\not{x}_{12} - \not{x}_{12}\not{\epsilon})\lambda_2 \frac{(x_{12}\cdot z)^{s-1}}{|x_{12}|^{2\Delta_\psi-\tau}}, \tag{B10}$$

which, it turns out, does not mix with v_{b_1}.

2. Integration kernel

Using the above results, we compute the integration kernel as usual.

For parity-even spin-s operators, the diagrammatic equation in Fig. 3 of the main text translates into the eigenvalue equation for the coefficients a_1, a_2 and c_1 defined in Eqs. (B2) and (B4):

$$\begin{pmatrix} a_1 \\ a_2 \\ c_1 \end{pmatrix} = \mathbf{K}^{\text{even}}_s(\tau) \begin{pmatrix} a_1 \\ a_2 \\ c_1 \end{pmatrix}. \tag{B11}$$

We must determine the values of τ for which the 3×3 matrix $\mathbf{K}^{\text{even}}_s(\tau)$ has an eigenvalue equal to 1. Similarly, for the spectrum of parity-odd spin-s operators, Fig. 3 of the main text translates into an eigenvalue equation for a 2×2 matrix $\mathbf{K}^{\text{odd}}_s(\tau)$. For parity-even spin zero operators, Fig. 3 of the main text translates into an eigenvalue equation for another 2×2 matrix, $\mathbf{K}^{\text{even}}_0(\tau)$. For parity-odd spin-zero operators, Fig. 3 of the main text translates into a conventional integration kernel, i.e., a 1×1 matrix, $K^{\text{odd}}_0(\tau)$.

The nine entries of the integration kernel matrix for spin-s parity-even operators are given by

$$\mathbf{K}^{\text{even}}_s(\tau) = \begin{pmatrix} K_{a_1,a_1}[v_{a_1}(y_1,y_2)]/v_{a_1}(x_1,x_2) & K_{a_1,a_2}[v_{a_2}(y_1,y_2)]/v_{a_1}(x_1,x_2) & K_{a_1,c}[v_c(y_1,y_2)]/v_{a_1}(x_1,x_2) \\ K_{a_2,a_1}[v_{a_1}(y_1,y_2)]/v_{a_2}(x_1,x_2) & K_{a_2,a_2}[v_{a_2}(y_1,y_2)]/v_{a_2}(x_1,x_2) & K_{a_2,c}[v_c(y_1,y_2)]/v_{a_2}(x_1,x_2) \\ K_{c,a_1}[v_{a_1}(y_1,y_2)]/v_c(x_1,x_2) & K_{c,a_2}[v_{a_2}(y_1,y_2)]/v_c(x_1,x_2) & K_{c,c}[v_c(y_1,y_2)]/v_c(x_1,x_2) \end{pmatrix}, \tag{B12}$$

for $s > 0$. For s odd, the last row and last column of this matrix vanish identically. For $s = 0$, the second row and second column of the matrix are not present.

The four entries of the integration kernel matrix for spin-zero parity-even operators are given by

$$\mathbf{K}^{\text{even}}_0(\tau) = \begin{pmatrix} K_{a_1,a_1}[v_{a_1}(y_1,y_2)]/v_{a_1}(x_1,x_2) & K_{a_1,c}[v_c(y_1,y_2)]/v_{a_1}(x_1,x_2) \\ K_{c,a_1}[v_{a_1}(y_1,y_2)]/v_c(x_1,x_2) & K_{c,c}[v_c(y_1,y_2)]/v_c(x_1,x_2) \end{pmatrix}, \tag{B13}$$

for $s = 0$.

In the above matrices, we have

$$K_{a_1,a_1}[v_{a_1}(y_1,y_2)] + K_{a_2,a_1}[v_{a_1}(y_1,y_2)] = J\lambda \int d^d y_1 d^d y_2 \bar{\lambda}_1 G(x_1,y_1) \not{y}_{12} G(y_2,x_2) \lambda_2 \frac{(y_{12}\cdot\epsilon)^s}{y_{12}^{-\tau+1+2\Delta_\psi}} F(y_1,y_2), \tag{B14}$$

$$K_{c,a_1}[v_{a_1}(y_1,y_2)] = -J \int d^d y_1 d^d y_2 F(x_1,y_1) F(y_2,x_2) \mathrm{tr}(\not{y}_{12} G(y_2,y_1)) \frac{(y_{12}\cdot\epsilon)^s}{y_{12}^{-\tau+1+2\Delta_\psi}}, \tag{B15}$$

$$K_{a_1,a_2}[v_{a_2}(y_1,y_2)] + K_{a_2,a_2}[v_{a_2}(y_1,y_2)] = J\lambda \int d^d y_1 d^d y_2 \bar{\lambda}_1 G(x_1,y_1) \not{\epsilon} G(y_2,x_2) \lambda_2 \frac{(y_{12}\cdot\epsilon)^{s-1}}{y_{12}^{-\tau-1+2\Delta_\psi}} F(y_1,y_2), \tag{B16}$$

$$K_{c,a_2}[v_{a_2}(y_1,y_2)] = -J \int d^d y_1 d^d y_2 F(x_1,y_1) F(y_2,x_2) \mathrm{tr}(\not{\epsilon} G(y_2,y_1)) \frac{(y_{12}\cdot\epsilon)^{s-1}}{y_{12}^{-\tau-1+2\Delta_\psi}}, \tag{B17}$$

$$K_{a_1,c}[v_c(y_1,y_2)] + K_{a_2,c}[v_c(y_1,y_2)] = J\lambda \int d^d y_1 d^d y_2 \bar{\lambda}_1 G(x_1,y_1) G(y_1,y_2) G(y_2,x_2) \lambda_2 \frac{(y_{12}\cdot\epsilon)^s}{y_{12}^{-\tau+2\Delta_\sigma}}, \tag{B18}$$

and

$$K_{c,c}[v_c(y_1,y_2)] = 0. \tag{B19}$$

For parity-odd spin-s operators, we have

$$\mathbf{K}_s^{\mathrm{odd}}(\tau) = \begin{pmatrix} K_{b_1,b_1}[v_{b_1}(y_1,y_2)]/v_{b_1}(x_1,x_2) & K_{b_1,b_2}[v_{b_2}(y_1,y_2)]/v_{b_1}(x_1,x_2) \\ K_{b_2,b_1}[v_{b_1}(y_1,y_2)]/v_{b_2}(x_1,x_2) & K_{b_2,b_2}[v_{b_2}(y_1,y_2)]/v_{b_2}(x_1,x_2) \end{pmatrix}, \tag{B20}$$

where

$$K_{b_1,b_1}[v_{b_1}(y_1,y_2)] + K_{b_2,b_1}[v_{b_1}(y_1,y_2)] = J\lambda \int d^d y_1 d^d y_2 \bar{\lambda}_1 G(x_1,y_1) G(y_2,x_2) \lambda_2 \frac{(y_{12}\cdot\epsilon)^s}{y_{12}^{-\tau+2\Delta_\psi}} F(y_1,y_2), \tag{B21}$$

and

$$K_{b_1,b_2}[v_{b_2}(y_1,y_2)] + K_{b_2,b_2}[v_{b_2}(y_1,y_2)] = J\lambda \int d^d y_1 d^d y_2 \bar{\lambda}_1 G(x_1,y_1) \not{\epsilon} \not{y}_{12} G(y_2,x_2) \lambda_2 \frac{(y_{12}\cdot\epsilon)^{s-1}}{y_{12}^{-\tau+2\Delta_\psi}} F(y_1,y_2). \tag{B22}$$

$\mathbf{K}_s^{\mathrm{odd}}(\tau)$ is a 2×2 matrix for $s > 0$. For parity-odd spin-0 operators, there is no mixing and only one allowed form for the three-point function. The integration kernel $K_0^{\mathrm{odd}}(\tau)$ is therefore a 1×1 matrix:

$$K_0^{\mathrm{odd}}(\tau) = K_{b_1,b_1}[v_{b_1}(y_1,y_2)]/v_{b_1}(x_1,x_2). \tag{B23}$$

Before we proceed, let us point out a technical complication. Unlike the usual SYK model, or the higher-dimensional bosonic variants, we find that there are multiple allowed forms for the three-point correlation functions. Like mixing, as discussed in [44,48,51], this means the integration kernel is a matrix—and the allowed scaling dimensions are those for which is 1 eigenvalue of the matrix. When two operators mix we expect two linearly independent mixtures to exist that have well-defined scaling dimensions. This is reflected in the fact that the calculation of the integration kernel involves diagonalizing a two-by-two matrix and eventually leads to two sets of spectra, both of which are physical. However, suppose there are multiple allowed forms for the three-point correlation function—for simplicity, assume that there are n allowed forms for the three-point function and no mixing. In the actual IR fixed point, only one three-point function would be realized, which corresponds to one of the eigenvectors of an $n\times n$ integration-kernel matrix, with eigenvalue 1. The other eigenvectors, and their associated eigenvalues, would be spurious. We therefore determine n candidate scaling

dimensions for each operator, without identifying which of these scaling dimensions is actually realized. Luckily, we are able to resolve this ambiguity by assuming the spectrum of the theory is a continuous function of λ. This complication does not affect spin-zero operators.

3. Numerically solving for the allowed scaling dimensions

To determine the allowed scaling dimensions of parity-odd scalars, we must determine the values of $\tilde{\Delta}$ for which $K_0^{\text{odd}}(\tilde{\Delta}) = 1$. This gives rise to

$$-\frac{\Gamma(\frac{1}{2}(d-2\Delta_\psi+1))\Gamma(d-\Delta_\psi+\frac{1}{2})\Gamma(\Delta_\psi-\frac{\tilde{\Delta}}{2})\Gamma(-\frac{d}{2}+s+\Delta_\psi+\frac{\tilde{\Delta}}{2})}{\Gamma(\Delta_\psi+\frac{1}{2})\Gamma(-\frac{d}{2}+\Delta_\psi+\frac{1}{2})\Gamma(d-\Delta_\psi-\frac{\tilde{\Delta}}{2})\Gamma(\frac{1}{2}(d+2s-2\Delta_\psi+\tilde{\Delta}))}=1. \tag{B24}$$

We carry out this computation numerically for $d = 3$, as illustrated in Figs. 10 and 11 for $\lambda = 1$ and $\lambda = \infty$, respectively. These figures illustrate that the spectrum is real for these values of λ, and we established analytically that the spectrum is real for small λ. We also determined the spectrum for numerous intermediate values of λ and found that it is real as well.

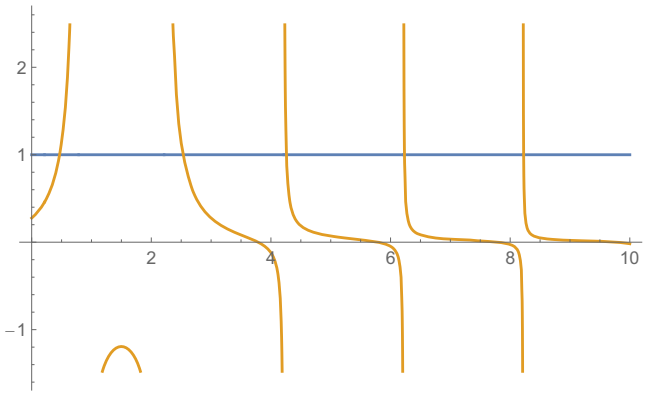

FIG. 10. Computing the spectrum of spin-zero parity-odd scalars in $d = 3$ for $\lambda = 1$. For other values of λ, the calculation is very similar, and we find the lowest twist parity-odd scalar has real scaling dimension for all λ, in contrast to other nonsupersymmetric melonic theories, such as [50].

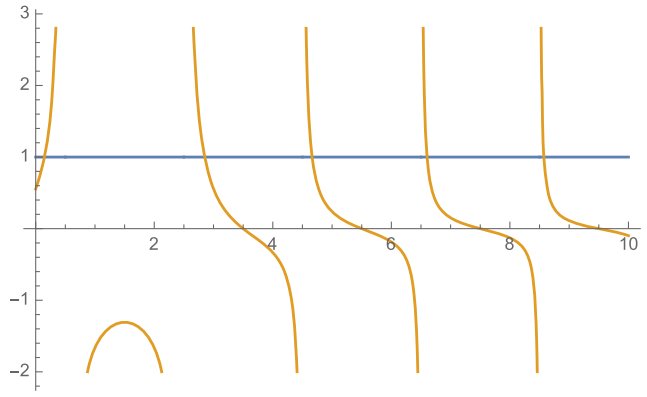

FIG. 11. Computing the spectrum of spin-zero parity-odd scalars in $d = 3$ for $\lambda = \infty$.

Let us discuss a potential concern regarding the spectrum. When $\lambda = 0$ the disordered spectrum is that of the large-N GN model. One might also expect that the $O(\lambda^1)$ correction to the disordered spectrum matches the $O(1/N)$ correction to the spectrum of the GN model, but this is not quite true. The $1/N$ contribution to scaling dimension of the single-trace scalar primary in the GN model is $\tilde{\Delta}_0' = 1 - \frac{16}{3\pi^2}\frac{1}{N}$, which is the shadow of the value quoted for $\tilde{\Delta}_0$ above when λ is replaced by $1/N$. The reason for this discrepancy is as follows. When $M = 1$, in the GN model, the scalar field σ can be integrated out, and its equation of motion sets $\bar{\psi}\psi = 0$, effectively replacing the scalar primary with σ. When one computes the $1/N$ anomalous dimension of σ in the GN model, using e.g., Feynman diagrams, one obtains the correction $-\frac{16}{3\pi^2}\frac{1}{N}$, leading to the value Δ_0' quoted above. However, in the disordered theory with $M > 1$, we cannot integrate out σ, so we cannot set $\bar{\psi}\psi$ to zero—its scaling dimension becomes meaningful, and is equal to $\tilde{\Delta}_0$ computed above for any $\lambda > 0$. The order λ correction to the scaling dimension of σ^a also does not match the $1/N$ correction to the scaling dimension of σ in the GN model—this is because the Feynman diagrams that contribute to the $1/N$ anomalous dimension of σ in the GN model include a nonmelonic diagram that is suppressed by $1/N$ rather than M/N in the disordered theory.

APPENDIX C: HIGHER-TWIST SPIN-s OPERATORS IN $d = 3$

1. Parity-even higher-spin operators

The calculation leading to the numerical spectrum for $s = 1, 2$ and $\lambda = 1$ is shown in Fig. 12. The plots for higher-spin operators are similar, except that the leading twist is no longer at $\tau = 1$.

From Fig. 12, we see that, for operators of both leading and subleading twist, there is no ambiguity in the spectrum. The spectrum of operators of subleading twists is shown in Fig. 13 as a function of λ.

However, as discussed in Appendix B, there is an ambiguity in determining the higher-twist higher-spin operators. Because there are two allowed forms for the correlation function involving two fermions and a spin-s

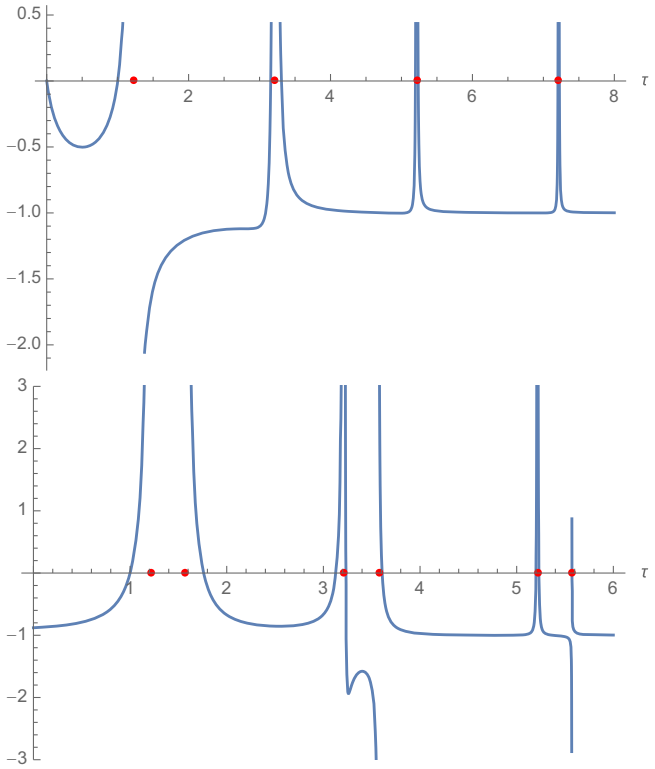

FIG. 12. Determining the spectrum of parity-even single-trace spin-1 (above) and spin-2 (below) operators for $\lambda = 1$. Red dots denote asymptotic values of twists, approached as $n \to \infty$.

operator, we find two values of $\tau^{A}_{s,n}$ for which $K = 1$, for each $s > 0$ and $n > 0$. These approach $2\Delta_\psi - 1$ from above and below as $n \to \infty$ or $s \to \infty$, so we denote them as $\tau^{A+}_{s,n}$ and $\tau^{A-}_{s,n}$, respectively. Only one of $\tau^{A\pm}_{s,n}$ is physical. Because there is only one allowed form for $\langle \sigma\sigma J_s \rangle$, no such ambiguity is present for $\tau^{B}_{s,n}$. This can be seen in Fig. 12.

We resolve this ambiguity by demanding anomalous dimensions are continuous functions of λ. We find that the functions

$$\tau^{(1)}_{s,n}(\lambda) = \begin{cases} \tau^{A-}_{s,n}(\lambda) & \lambda < \lambda_* \\ \tau^{B}_{s,n}(\lambda) & \lambda > \lambda_* \end{cases} \tag{C1}$$

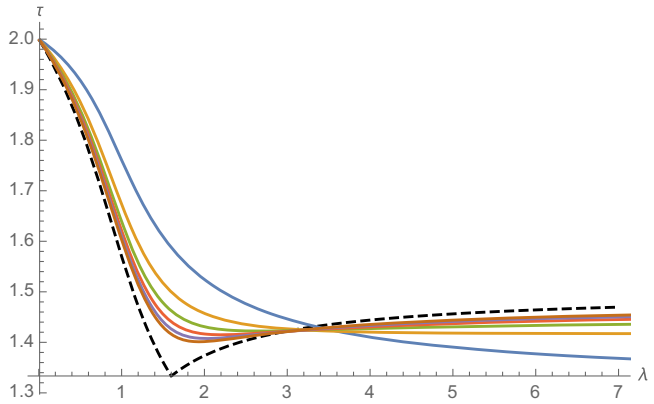

FIG. 13. The anomalous dimensions of the even spin higher-spin operators of subleading twist. The dashed line is the asymptotic value approached as $s \to \infty$. For sufficiently large λ these are monotonically increasing functions of s.

and

$$\tau^{(2)}_{s,n}(\lambda) = \begin{cases} \tau^{B}_{s,n}(\lambda) & \lambda < \lambda_* \\ \tau^{A+}_{s,n}(\lambda) & \lambda > \lambda_* \end{cases} \tag{C2}$$

are continuous functions of λ. Therefore

$$\tau^{A}_{n,s} = \begin{cases} \tau^{A-}_{n,s} & \lambda < \lambda* \\ \tau^{A+}_{n,s} & \lambda > \lambda* . \end{cases} \tag{C3}$$

2. Parity-odd higher-spin operators

The same ambiguity arises for parity-odd higher-spin operators. In this case, it is possible to explicitly choose a basis—formed by v_{b_1} and v'_{b_2} in Eqs. (B7) and (B10)—for correlation functions that diagonalizes the 2×2 integration kernel matrix for all Δ_ψ, τ and s. There are therefore two integration kernels:

$$\tilde{K}^{+}_{s}(\tilde{\tau}) = -\frac{\Gamma(\frac{1}{2}(d-2\Delta_\psi+1))\Gamma(d-\Delta_\psi+\frac{1}{2})\Gamma(\Delta_\psi-\frac{\tau}{2})\Gamma(-\frac{d}{2}+s+\Delta_\psi+\frac{\tau}{2})}{\Gamma(\Delta_\psi+\frac{1}{2})\Gamma(-\frac{d}{2}+\Delta_\psi+\frac{1}{2})\Gamma(d-\Delta_\psi-\frac{\tau}{2})\Gamma(\frac{1}{2}(d+2s-2\Delta_\psi+\tau))}, \tag{C4}$$

and

$$\tilde{K}^{-}_{s}(\tilde{\tau}) = \frac{2\Gamma(\frac{1}{2}(d-2\Delta_\psi+1))\Gamma(d-\Delta_\psi+\frac{1}{2})\Gamma(\Delta_\psi-\frac{\tau}{2})\Gamma(-\frac{d}{2}+s+\Delta_\psi+\frac{\tau}{2})}{\Gamma(\Delta_\psi+\frac{1}{2})\Gamma(-\frac{d}{2}+\Delta_\psi+\frac{1}{2})\Gamma(d-\Delta_\psi-\frac{\tau}{2})\Gamma(\frac{1}{2}(d+2s-2\Delta_\psi+\tau))}. \tag{C5}$$

The eigenvector corresponding to $\tilde{K}_s^+$ is v_{b_1}, is also valid for $s=0$, while the eigenvector corresponding to $\tilde{K}_s^-$ is v'_{b_2} and requires $s \geq 1$.

The equations $\tilde{K}_s^{\pm}(\tilde{\tau}) = 1$ have solutions $\tilde{\tau}_{n,s}^+$ and $\tilde{\tau}_{n,s}^-$ for each integer $n \geq 0$. $\tilde{\tau}_{n,s}^+$ and $\tilde{\tau}_{n,s}^-$ approach $2\Delta_\psi + 2n$ from above and below, respectively, as $n \to \infty$ or $s \to \infty$.

When we solve these equations numerically, we find that $\tilde{\tau}_{1,0}^-(\lambda)$ becomes complex near $\lambda = 6.375$, while $\tilde{\tau}_{s,0}^+$ remains real for all λ. Hence, it is important to know whether $\tilde{\tau}_{s,n}^+$ or $\tilde{\tau}_{s,n}^-$ is realized in the IR limit.

We carried out a perturbative Feynman diagram calculation of the anomalous dimension of $\bar{\psi} \overleftrightarrow{\partial}(\cdot z)^s \psi$ to first order in λ for odd s. This is very similar to calculating $1/N$ corrections to the GN vector model, we use the IR propagators at $\lambda = 0$: $F(p) = \frac{8\lambda}{Jp}$ and $G(p) = G_0(p)$, and keep track of index contractions arising from disorder averaging—which means we keep only melonic diagrams. There is only one diagram that contributes for odd s (other than the self-energy of the fermion) which is given by

$$-\int \frac{d^3q}{(2\pi)^3} \frac{8\lambda}{q(p+q)^2} ((p+q)\cdot z)^s \to -\frac{4}{(2s+1)\pi^2} \lambda \log \Lambda. \tag{C6}$$

We find that $\tilde{\tau}_{s,0} = 2\Delta_\psi + \frac{4}{(2s+1)\pi^2}\lambda + O(\lambda^2)$, for odd s, which matches $\tilde{\tau}_{s,0}^+$ obtained from solving $\tilde{K}_s^+ = 1$. Assuming anomalous dimensions are continuous functions of λ, we conclude that $\tilde{\tau}_{s,0}^+$ are the physically realized twists for the leading-twist parity-odd higher-spin operators, and our spectrum is free from any operators of complex scaling dimension for all λ. If we assume $\tilde{\tau}_{s,n}$ are monotonic functions of n, this also implies that $\tau_{s,n}^+$ are the physically realized twists for $n > 0$—to confirm this expectation would require an order λ^2 perturbative calculation. However, for $n > 0$, both $\tau_{s,n}^+$ and $\tau_{s,n}^-$ are real so distinguishing between them is not essential for the main conclusion of the paper.

For small λ, we find that

$$\tilde{\gamma}_{s,0} = \frac{4}{\pi^2(2s+1)}\lambda + \frac{16(9(2s+1)^2 H_{s-\frac{1}{2}} + 80s^3 + 12s^2(13+\log(64)) + 12s(8+\log(64)) - 8 + 9\log(4))}{27\pi^4(2s+1)^3}\lambda^2 + O(\lambda^3) \tag{C7}$$

and

$$\begin{aligned}\tilde{\gamma}_{s,n} &= \frac{16}{3\pi^4 n(2n+2s+1)}\lambda^2 + \frac{8(6n(2n+2s+1)(H_{n+s-\frac{1}{2}} + H_{n-1} + \log(4)) + 26n(2n+2s+1) + 9)}{27\pi^6 n^2 (n+s+\frac{1}{2})^2}\lambda^3 + O(\lambda^4) \\ &\sim_{n\to\infty} \frac{8}{3\pi^4 n^2}\lambda^2 + \frac{32(6\log(n) + 6\gamma + 13 + 3\log(4))}{27\pi^6 n^2}\lambda^3 + O(\lambda^3) \\ &\sim_{s\to\infty} \frac{8}{3\pi^4 ns}\lambda^2 + \frac{32(3H_{n-1} + 3\log(s) + 3\gamma + 13 + 3\log(4))}{27\pi^6 ns}\lambda^3 + O(\lambda^4).\end{aligned} \tag{C8}$$

At large s, we find

$$\tilde{\gamma}_{s,n} \sim \frac{2^{4\Delta_\psi - 5}(2\Delta_\psi - 5)\sin(2\pi\Delta_\psi)\Gamma(4-2\Delta_\psi)}{\pi(1-2\Delta_\psi)} s^{-\Delta_\sigma}, \tag{C9}$$

and at large n,

$$\tilde{\gamma}_{s,n} \sim \frac{2^{4\Delta_\psi - 5}(5-2\Delta_\psi)\sin^2(2\pi\Delta_\psi)\Gamma(3-2\Delta_\psi)\Gamma(4-2\Delta_\psi)}{\pi^2(2\Delta_\psi - 1)} \times n^{-2\Delta_\sigma}. \tag{C10}$$

APPENDIX D: SPECTRUM IN $d = 4 - \epsilon$

We also solve the spectrum of single-trace bilinears in the theory in $d = 4 - \epsilon$, which allows us to determine analytic expressions for various quantities in terms of λ. In this section, it is convenient to absorb d_γ into the definition of λ by defining $\hat{\lambda} = \frac{2M}{d_\gamma N}$; alternatively, one can set $d_\gamma = 2$ and then $\hat{\lambda} = \lambda$.

1. The gap equation

We first solve the gap equation. The allowed range for Δ_ψ is $\frac{3}{2} - \frac{\epsilon}{2} \leq \Delta_\psi \leq \frac{3}{2} - \frac{\epsilon}{4}$. We find

$$\Delta_\psi = \frac{3}{2} - \frac{(\hat{\lambda}+2)\epsilon}{4(\hat{\lambda}+1)} + \frac{\hat{\lambda}(5\hat{\lambda}-6)\epsilon^2}{32(\hat{\lambda}+1)^3} + O(\epsilon^3), \tag{D1}$$

and

$$\Delta_\sigma = 1 - \frac{\hat{\lambda}\epsilon}{2(\hat{\lambda}+1)} - \frac{\hat{\lambda}(5\hat{\lambda}-6)\epsilon^2}{16(\hat{\lambda}+1)^3} + O(\epsilon^3). \tag{D2}$$

The critical value, $\hat{\lambda}_*$, of $\hat{\lambda}$ at which $2\Delta_\psi(\hat{\lambda}_*) - 1 = 2\Delta_\sigma(\hat{\lambda}_*)$ is given by $\hat{\lambda}_* = 2 - \frac{\epsilon}{3} - \frac{\epsilon^2}{18} + O(\epsilon^3)$.

2. Parity-odd scalars

Solving for the spectrum of parity-odd scalars, we find the lowest scalar has scaling dimension given by

$$\tilde{\Delta}_0 = 3 + \frac{(\hat{\lambda}-2)\epsilon}{2(\hat{\lambda}+1)} - \frac{\hat{\lambda}(14\hat{\lambda}^2 - 5\hat{\lambda} + 14)\epsilon^2}{16(\hat{\lambda}+1)^3} + \frac{\hat{\lambda}(32\hat{\lambda}^4 - 57\hat{\lambda}^3 + 143\hat{\lambda}^2 - 153\hat{\lambda} - 22)\epsilon^3}{64(\hat{\lambda}+1)^5} + O(\epsilon^4). \tag{D3}$$

The higher-twist parity-odd scalars have dimension

$$\begin{aligned}\tilde{\Delta}_n = {} & 2\Delta_\psi + 2n + \frac{8\epsilon^2\hat{\lambda}^2(\hat{\lambda}+1)}{16(\hat{\lambda}+1)^3 n(n+1)} \\ & + \frac{\epsilon^3\hat{\lambda}^2(4\hat{\lambda}(\hat{\lambda}+1)(2n(n+1)H_{n-1}+1) + \hat{\lambda}^2(-7n^2+n+4) + \hat{\lambda}(n^2+13n+4) - 2n(7n+5))}{16(\hat{\lambda}+1)^4 n^2(n+1)^2} + O(\epsilon^4).\end{aligned} \tag{D4}$$

The anomalous dimensions for large n are

$$\tilde{\gamma}_{0,n} \sim \frac{\hat{\lambda}^2}{2(\hat{\lambda}+1)^2 n^2}\epsilon^2 + \frac{\hat{\lambda}^2(\hat{\lambda}(-7\hat{\lambda} + 8\gamma(\hat{\lambda}+1)+1) + 8\hat{\lambda}(\hat{\lambda}+1)\log n - 14)}{16(\hat{\lambda}+1)^4 n^2}\epsilon^3 + O(\epsilon^4), \tag{D5}$$

which is consistent with $\tilde{\gamma}_{0,n} \sim \frac{1}{n^{2\Delta_\sigma}}$.

3. Parity-even scalars

We next compute the parity-even scalar spectrum. We find for the lowest twist parity-even scalars

$$\Delta_0^A = 4 - \epsilon \tag{D6}$$

$$\begin{aligned}\Delta_0^B = {} & 2 - \frac{\left(\hat{\lambda} - \sqrt{\hat{\lambda}^2 + 14\hat{\lambda} + 1} + 1\right)\epsilon}{2\hat{\lambda}+2} - \frac{\hat{\lambda}(35\hat{\lambda}^2 - 5\hat{\lambda} + 26)\epsilon^2}{8((\hat{\lambda}+1)^3\sqrt{\hat{\lambda}^2+14\hat{\lambda}+1})} \\ & + \frac{3\hat{\lambda}(25\hat{\lambda}^6 + 136\hat{\lambda}^5 + 213\hat{\lambda}^4 + 3427\hat{\lambda}^3 + 336\hat{\lambda}^2 - 83\hat{\lambda} + 2)\epsilon^3}{32(\hat{\lambda}+1)^5(\hat{\lambda}^2+14\hat{\lambda}+1)^{3/2}} + O(\epsilon^4).\end{aligned} \tag{D7}$$

The anomalous dimensions of type-A higher twist parity-even scalars are

$$\begin{aligned}\gamma_{0,n}^A = {} & \frac{\hat{\lambda}^2\epsilon^2}{2(\hat{\lambda}+1)^2 n(n+2)} + \frac{\hat{\lambda}^2\epsilon^3}{16(\hat{\lambda}-2)(\hat{\lambda}+1)^4 n^2(n+1)^2(n+2)^2}(8\hat{\lambda}(\hat{\lambda}-2)(\hat{\lambda}+1)(n+1)^2(n+2)nH_{n-1} \\ & + 4(3\hat{\lambda}^3 + \hat{\lambda}^2 + 6\hat{\lambda} + 8) + (-7\hat{\lambda}^3 + 15\hat{\lambda}^2 - 16\hat{\lambda} + 28)n^4 - 4(4\hat{\lambda}^3 - 13\hat{\lambda}^2 + 23\hat{\lambda} - 26)n^3 \\ & + (5\hat{\lambda}^3 + 43\hat{\lambda}^2 - 168\hat{\lambda} + 124)n^2 + 2(13\hat{\lambda}^3 - 3\hat{\lambda}^2 - 58\hat{\lambda} + 24)n) + O(\epsilon^4) \\ \sim_{n\to\infty} {} & \epsilon^2\left(\frac{\hat{\lambda}^2}{2(\hat{\lambda}+1)^2 n^2}\right) + \epsilon^3\left(\frac{\hat{\lambda}^2(\hat{\lambda} - 7\hat{\lambda}^2 + 8\hat{\lambda}(\hat{\lambda}+1)(\log n + \gamma) - 14)}{16(\hat{\lambda}+1)^4 n^2}\right) + O(\epsilon^4),\end{aligned} \tag{D8}$$

which is consistent with $\gamma_{0,n}^A \sim n^{-2\Delta_\sigma}$ at large n. At finite n, the expression is slightly different when $\hat{\lambda} = \hat{\lambda}_*$.

For type-B scalars, the $n = 1$ operator needs to be handled separately:

$$\gamma_{0,1}^B = \frac{\hat{\lambda}}{\hat{\lambda}+1}\epsilon - \frac{\hat{\lambda}(\hat{\lambda}^2 + 8\hat{\lambda} + 18)}{8(\hat{\lambda}+1)^3}\epsilon^2 + O(\epsilon^3). \tag{D9}$$

For $\hat{\lambda} \neq \hat{\lambda}_*$, the type-B anomalous dimensions for $n > 1$ are

$$\gamma_{0,n}^B = -\frac{2\hat{\lambda}(\hat{\lambda}+2)}{(\hat{\lambda}-2)(\hat{\lambda}+1)^3 n^2(n^2-1)^2}\epsilon^3 + O(\epsilon^4), \tag{D10}$$

consistent with $\gamma_{0,n}^B \sim n^{-4\Delta_\psi}$.

For $\hat{\lambda} = \hat{\lambda}_* = 2 - \epsilon/3 - \epsilon^2/18$ the type-B anomalous dimensions for $n > 1$ are

$$\gamma^B_{0,n}(\hat{\lambda}_*) = \frac{n - \sqrt{n^2+8}}{9n(n+1)(n-1)}\epsilon^2 + O(\epsilon^3) \sim_{n\to\infty} -\frac{4}{9n^4}\epsilon^2 - \frac{2(4\log n + 4\gamma - 7)}{27n^4}\epsilon^3 + O(\epsilon^4), \tag{D11}$$

consistent with $\gamma^B_{0,n}(\hat{\lambda}_*) \sim n^{-(2\Delta_\psi+1)}$.

For type-A scalars, at $\hat{\lambda} = \hat{\lambda}_*$, the anomalous dimensions at finite n also differ from the results at generic values of $\hat{\lambda}$:

$$\gamma^A(\hat{\lambda}_*)_{0,n} = \frac{n + \sqrt{(n+1)^2+8} + 1}{9n(n+2)(n+3)}\epsilon + O(\epsilon)^2, \tag{D12}$$

but this does not affect the large n asymptotics.

4. Leading-twist higher-spin operators

Let us compute the leading-twist higher-spin operators, which are parity even.

For odd s, the leading twist of a spin-s operator with $s \geq 1$, is given by

$$\tau_{s,\min} = 2\Delta_\psi - 1 - \frac{\hat{\lambda}}{(\hat{\lambda}+1)(s^2+s)}\epsilon + \frac{\hat{\lambda}(-4\hat{\lambda}(\hat{\lambda}+1)((s+1)^2 s^2 H_{s-1}+1) + (7\hat{\lambda}^2+8\hat{\lambda}+12)s^4 + 2(3\hat{\lambda}^2+8)s^3 - \hat{\lambda}(\hat{\lambda}+12)s^2 - 4(\hat{\lambda}+1)(2\hat{\lambda}+1)s)}{8(\hat{\lambda}+1)^3 s^3 (s+1)^3}\epsilon^2 + O(\epsilon^3) = 2 - \frac{\epsilon(\hat{\lambda} + \frac{2\hat{\lambda}}{s^2+s} + 2)}{2(\hat{\lambda}+1)} + O(\epsilon^2). \tag{D13}$$

For s even, the leading twist of a spin-s operator with $s \geq 1$, is given by

$$\tau_{s,\min} = 2 - \frac{\epsilon(2\hat{\lambda} + \sqrt{\hat{\lambda}^2(s^2+s-2)^2 - 4\hat{\lambda}s(s^2+s-10)(s+1) + 4s^2(s+1)^2} + (3\hat{\lambda}+2)s(s+1))}{4(\hat{\lambda}+1)s(s+1)} + O(\epsilon^2). \tag{D14}$$

(We also computed the order ϵ^2 term for finite s, but we do not reproduce it here.) Equation (D14) is plotted in Fig. 14.

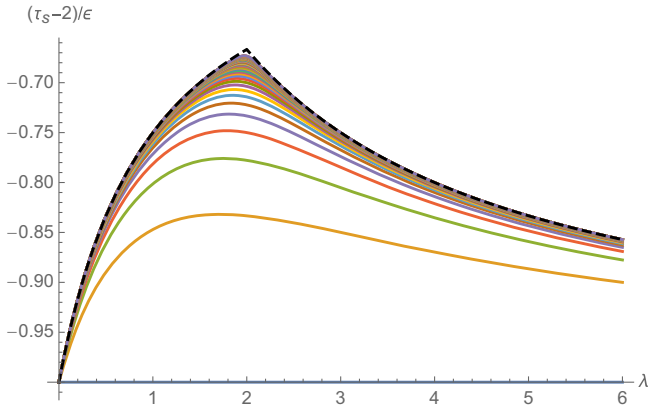

FIG. 14. The $O(\epsilon)$ contribution to the twist of leading-twist higher-spin operators in $d = 4 - \epsilon$, given in Eq. (D14) is plotted for even spins 2, 4,…, 100. The dashed line is the asymptotic behavior as $s \to \infty$.

The large s behavior of $\tau_{s,\min}$ for s odd is

$$\gamma_s = -\frac{\hat{\lambda}\epsilon}{(\hat{\lambda}+1)s^2} - \frac{\hat{\lambda}\epsilon^2((4\gamma-7)\hat{\lambda}^2 + 4(\gamma-2)\hat{\lambda} + 4(\hat{\lambda}+1)\hat{\lambda}\log(s) - 12)}{8(\hat{\lambda}+1)^3 s^2} + O(\epsilon^3) = -\frac{\hat{\lambda}\epsilon}{(\hat{\lambda}+1)s^2} - \frac{\epsilon^2\hat{\lambda}^2\log s}{2(\hat{\lambda}+1)^2 s^2} + O(\epsilon^3). \tag{D15}$$

The smallest twist operator is the stress tensor, which has twist $2 - \epsilon$. However, all higher-spin operators have twists $2 + O(\epsilon)$, and would also contribute to the term of order $\epsilon^2 s^{-2}\log s$ in the above expression.

For operators with even spin, the large-spin behavior of anomalous dimensions depends on whether or not $\hat{\lambda}$ exceeds $\hat{\lambda}_*$. For $\hat{\lambda} < 2 - \epsilon/3$, the large spin anomalous dimensions, including ϵ^2 terms, are

$$\gamma_s \sim -\frac{(\hat{\lambda}-6)\hat{\lambda}\epsilon}{(\hat{\lambda}-2)(\hat{\lambda}+1)s^2}+\frac{\hat{\lambda}(\hat{\lambda}^2-6\hat{\lambda}-8)}{2(\hat{\lambda}-2)(\hat{\lambda}+1)^2s^2}\epsilon^2\log s + O(\epsilon^3) \tag{D16}$$

and, for $\hat{\lambda} > 2-\epsilon/3$,

$$\gamma_s \sim -\frac{4\hat{\lambda}\epsilon}{(\hat{\lambda}-2)(\hat{\lambda}+1)s^2}+\frac{2\hat{\lambda}(\hat{\lambda}+2)}{(\hat{\lambda}-2)(\hat{\lambda}+1)^2s^2}\epsilon^2\log s + O(\epsilon^3). \tag{D17}$$

Above, we only included terms of order $\epsilon^n(\log s)^{n-1}$. These expressions are consistent with the exchange of multiple operators with twists of order $2+O(\epsilon)$ in the four-point function.

The order ϵ^2 correction to γ_s for $\hat{\lambda} = 2-\epsilon/3$ is

$$\gamma_s|_{\hat{\lambda}=\hat{\lambda}_*} = -\frac{2}{3s}\epsilon + \left(\frac{7s^4+8s^3-9s^2-9s-2}{9s^3(s+1)(2s+1)}-\frac{2H_{s-1}}{9s}\right)\epsilon^2+O(\epsilon^3) \to -\frac{2}{3s}\epsilon+\left(\frac{-4\log(s)-4\gamma+7}{18s}\right)\epsilon^2+O(\epsilon^3). \tag{D18}$$

This is consistent with

$$\gamma_s \sim \left(-\frac{2}{3}\epsilon\right)s^{-(1-\frac{\epsilon}{3})} = \left(-\frac{2}{3}\epsilon\right)s^{-\Delta_\sigma}, \tag{D19}$$

as would arise from exchange of the scalar field σ^a. It would be interesting to understand the large spin behavior of the theory at $\hat{\lambda}_*$ better via analytic bootstrap methods [94–99], assuming they can also be applied to the present disordered CFT, which appears to be unitary.

[1] G. 't Hooft, Nucl. Phys. **B72**, 461 (1974).
[2] J. M. Maldacena, Adv. Theor. Math. Phys. **2**, 231 (1998).
[3] S. Gubser, I. R. Klebanov, and A. M. Polyakov, Phys. Lett. B **428**, 105 (1998).
[4] E. Witten, Adv. Theor. Math. Phys. **2**, 253 (1998).
[5] G. 't Hooft, Nucl. Phys. **B75**, 461 (1974).
[6] I. Klebanov and A. Polyakov, Phys. Lett. B **550**, 213 (2002).
[7] E. Sezgin and P. Sundell, J. High Energy Phys. 07 (2005) 044.
[8] R. G. Leigh and A. C. Petkou, J. High Energy Phys. 06 (2003) 011.
[9] S. Giombi, S. Minwalla, S. Prakash, S. P. Trivedi, S. R. Wadia, and X. Yin, Eur. Phys. J. C **72**, 2112 (2012).
[10] O. Aharony, G. Gur-Ari, and R. Yacoby, J. High Energy Phys. 03 (2012) 037.
[11] J. Maldacena and A. Zhiboedov, J. Phys. A **46**, 214011 (2013).
[12] J. Maldacena and A. Zhiboedov, Classical Quantum Gravity **30**, 104003 (2013).
[13] O. Aharony, O. Bergman, D. L. Jafferis, and J. Maldacena, J. High Energy Phys. 10 (2008) 091.
[14] O. Aharony, O. Bergman, and D. L. Jafferis, J. High Energy Phys. 11 (2008) 043.
[15] C.-M. Chang, S. Minwalla, T. Sharma, and X. Yin, J. Phys. A **46**, 214009 (2013).
[16] H. Ooguri and C. Vafa, Adv. Theor. Math. Phys. **21**, 1787 (2017).
[17] V. Gurucharan and S. Prakash, J. High Energy Phys. 09 (2014) 009; 11 (2017) 045(E).
[18] S. Kapoor and S. Prakash, arXiv:2112.01055.
[19] H. Osborn and A. Stergiou, J. High Energy Phys. 05 (2018) 051.
[20] V. Guru Charan and S. Prakash, J. High Energy Phys. 02 (2018) 094.
[21] R. Gurau, Commun. Math. Phys. **304**, 69 (2011).
[22] R. Gurau and V. Rivasseau, Europhys. Lett. **95**, 50004 (2011).
[23] R. Gurau, Ann. Inst. Henri Poincaré **13**, 399 (2012).
[24] V. Bonzom, R. Gurau, A. Riello, and V. Rivasseau, Nucl. Phys. **B853**, 174 (2011).
[25] A. Tanasa, J. Phys. A **45**, 165401 (2012).
[26] V. Bonzom, R. Gurau, and V. Rivasseau, Phys. Rev. D **85**, 084037 (2012).
[27] S. Carrozza and A. Tanasa, Lett. Math. Phys. **106**, 1531 (2016).
[28] E. Witten, J. Phys. A **52**, 474002 (2019).
[29] I. R. Klebanov and G. Tarnopolsky, Phys. Rev. D **95**, 046004 (2017).
[30] S. Prakash and R. Sinha, Phys. Rev. D **101**, 126001 (2020).
[31] S. Sachdev and J. Ye, Phys. Rev. Lett. **70**, 3339 (1993).
[32] A. Kitaev, A simple model of quantum holography (2015), http://online.kitp.ucsb.edu/online/entangled15/kitaev/; http://online.kitp.ucsb.edu/online/entangled15/kitaev2/.
[33] J. Maldacena and D. Stanford, Phys. Rev. D **94**, 106002 (2016).
[34] A. Kitaev and S. J. Suh, J. High Energy Phys. 05 (2018) 183.
[35] V. Rosenhaus, J. Phys. A **52**, 323001 (2019).
[36] W. Fu, D. Gaiotto, J. Maldacena, and S. Sachdev, Phys. Rev. D **95**, 026009 (2017); **95**, 069904(A) (2017).
[37] A. Jevicki, K. Suzuki, and J. Yoon, J. High Energy Phys. 07 (2016) 007.
[38] G. Mandal, P. Nayak, and S. R. Wadia, J. High Energy Phys. 11 (2017) 046.

[39] S. R. Das, A. Jevicki, and K. Suzuki, J. High Energy Phys. 09 (2017) 017.
[40] S. R. Das, A. Ghosh, A. Jevicki, and K. Suzuki, J. High Energy Phys. 02 (2018) 162.
[41] K. Bulycheva, I. R. Klebanov, A. Milekhin, and G. Tarnopolsky, Phys. Rev. D **97**, 026016 (2018).
[42] D. J. Gross and V. Rosenhaus, J. High Energy Phys. 05 (2017) 092.
[43] G. Turiaci and H. Verlinde, J. High Energy Phys. 10 (2017) 167.
[44] J. Murugan, D. Stanford, and E. Witten, J. High Energy Phys. 08 (2017) 146.
[45] J. Liu, E. Perlmutter, V. Rosenhaus, and D. Simmons-Duffin, J. High Energy Phys. 03 (2019) 052.
[46] C. Peng, J. High Energy Phys. 12 (2018) 065.
[47] C.-M. Chang, S. Colin-Ellerin, C. Peng, and M. Rangamani, J. High Energy Phys. 11 (2021) 211.
[48] C.-M. Chang, S. Colin-Ellerin, C. Peng, and M. Rangamani, Phys. Rev. Lett. **129**, 011603 (2022).
[49] S. Giombi, I. R. Klebanov, and G. Tarnopolsky, Phys. Rev. D **96**, 106014 (2017).
[50] S. Prakash and R. Sinha, J. High Energy Phys. 02 (2018) 086.
[51] S. Giombi, I. R. Klebanov, F. Popov, S. Prakash, and G. Tarnopolsky, Phys. Rev. D **98**, 105005 (2018).
[52] J. Kim, E. Altman, and X. Cao, Phys. Rev. B **103**, 081113 (2021).
[53] D. J. Gross and A. Neveu, Phys. Rev. D **10**, 3235 (1974).
[54] D. Benedetti, S. Carrozza, R. Gurau, and A. Sfondrini, J. High Energy Phys. 01 (**2018**) 003.
[55] D. Benedetti, R. Gurau, and S. Harribey, J. High Energy Phys. 06 (2019) 053.
[56] A. Hasenfratz, P. Hasenfratz, K. Jansen, J. Kuti, and Y. Shen, Nucl. Phys. **365**, 79 (1991).
[57] J. Zinn-Justin, Nucl. Phys. **B367**, 105 (1991).
[58] M. Moshe and J. Zinn-Justin, Phys. Rep. **385**, 69 (2003).
[59] L. Fei, S. Giombi, I. R. Klebanov, and G. Tarnopolsky, Prog. Theor. Exp. Phys. **2016**, 12C105 (2016).
[60] T. Muta and D. S. Popovic, Prog. Theor. Phys. **57**, 1705 (1977).
[61] W. Wetzel, Phys. Lett. **153B**, 297 (1985).
[62] J. A. Gracey, Int. J. Mod. Phys. A **06**, 395 (1991); **06**, 2755(E) (1991).
[63] J. Zinn-Justin, Nucl. Phys. **B367**, 105 (1991).
[64] J. A. Gracey, Nucl. Phys. **B367**, 657 (1991).
[65] C. Luperini and P. Rossi, Ann. Phys. (N.Y.) **212**, 371 (1991).
[66] A. N. Vasiliev, S. E. Derkachov, N. A. Kivel, and A. S. Stepanenko, Theor. Math. Phys. **94**, 127 (1993).
[67] J. A. Gracey, Phys. Lett. B **297**, 293 (1992).
[68] N. A. Kivel, A. S. Stepanenko, and A. N. Vasiliev, Nucl. Phys. **B424**, 619 (1994).
[69] J. A. Gracey, Int. J. Mod. Phys. A **09**, 727 (1994).
[70] S. E. Derkachov, N. A. Kivel, A. S. Stepanenko, and A. N. Vasiliev, arXiv:hep-th/9302034.
[71] J. A. Gracey, Nucl. Phys. **B802**, 330 (2008).
[72] A. Raju, J. High Energy Phys. 10 (2016) 097.
[73] S. Ghosh, R. K. Gupta, K. Jaswin, and A. A. Nizami, J. High Energy Phys. 03 (**2016**) 174.
[74] A. N. Manashov and E. D. Skvortsov, J. High Energy Phys. 01 (2017) 132.
[75] J. A. Gracey, T. Luthe, and Y. Schroder, Phys. Rev. D **94**, 125028 (2016).
[76] S. Giombi, V. Kirilin, and E. Skvortsov, J. High Energy Phys. 05 (2017) 041.
[77] C. Cresswell-Hogg and D. F. Litim, arXiv:2207.10115.
[78] B. Kang and J. Yoon, Phys. Rev. B **105**, 045117 (2022).
[79] J. Kim, X. Cao, and E. Altman, Phys. Rev. B **101**, 125112 (2020).
[80] Y. Wang, Phys. Rev. Lett. **124**, 017002 (2020).
[81] I. Esterlis and J. Schmalian, Phys. Rev. B **100**, 115132 (2019).
[82] E. Marcus and S. Vandoren, J. High Energy Phys. 01 (2019) 166.
[83] Z. Bi, C.-M. Jian, Y.-Z. You, K. A. Pawlak, and C. Xu, Phys. Rev. B **95**, 205105 (2017).
[84] V. Bonzom, V. Nador, and A. Tanasa, Lett. Math. Phys. **109**, 2611 (2019).
[85] S. Giombi, S. Prakash, and X. Yin, J. High Energy Phys. 07 (2013) 105.
[86] S. Giombi and V. Kirilin, J. High Energy Phys. 11 (2016) 068.
[87] J. Polchinski and V. Rosenhaus, J. High Energy Phys. 04 (2016) 001.
[88] D. J. Gross and V. Rosenhaus, J. High Energy Phys. 02 (2017) 093.
[89] D. Chowdhury and E. Berg, Ann. Phys. (Amsterdam) **417**, 168125 (2020).
[90] Y. Wang and A. V. Chubukov, Phys. Rev. Res. **2**, 033084 (2020).
[91] I. Esterlis, H. Guo, A. A. Patel, and S. Sachdev, Phys. Rev. B **103**, 235129 (2021).
[92] J. Kim, I. R. Klebanov, G. Tarnopolsky, and W. Zhao, Phys. Rev. X **9**, 021043 (2019).
[93] I. R. Klebanov, A. Milekhin, G. Tarnopolsky, and W. Zhao, J. High Energy Phys. 11 (2020) 162.
[94] L. F. Alday and J. M. Maldacena, J. High Energy Phys. 11 (2007) 019.
[95] Z. Komargodski and A. Zhiboedov, J. High Energy Phys. 11 (2013) 140.
[96] A. L. Fitzpatrick, J. Kaplan, D. Poland, and D. Simmons-Duffin, J. High Energy Phys. 12 (2013) 004.
[97] R. Gopakumar, A. Kaviraj, K. Sen, and A. Sinha, Phys. Rev. Lett. **118**, 081601 (2017).
[98] P. Dey, A. Kaviraj, and A. Sinha, J. High Energy Phys. 07 (2017) 019.
[99] A. Bissi, A. Sinha, and X. Zhou, Phys. Rep. **991**, 1 (2022).